

PPPL- 5155

Ideal plasma response to vacuum magnetic fields with resonant magnetic perturbations in non-axisymmetric tokamaks

Kimin Kim, J. W. Ahn, F. Scotti, J. K. Park and J. E. Menard

July 2015



Princeton Plasma Physics Laboratory

Report Disclaimers

Full Legal Disclaimer

This report was prepared as an account of work sponsored by an agency of the United States Government. Neither the United States Government nor any agency thereof, nor any of their employees, nor any of their contractors, subcontractors or their employees, makes any warranty, express or implied, or assumes any legal liability or responsibility for the accuracy, completeness, or any third party's use or the results of such use of any information, apparatus, product, or process disclosed, or represents that its use would not infringe privately owned rights. Reference herein to any specific commercial product, process, or service by trade name, trademark, manufacturer, or otherwise, does not necessarily constitute or imply its endorsement, recommendation, or favoring by the United States Government or any agency thereof or its contractors or subcontractors. The views and opinions of authors expressed herein do not necessarily state or reflect those of the United States Government or any agency thereof.

Trademark Disclaimer

Reference herein to any specific commercial product, process, or service by trade name, trademark, manufacturer, or otherwise, does not necessarily constitute or imply its endorsement, recommendation, or favoring by the United States Government or any agency thereof or its contractors or subcontractors.

PPPL Report Availability

Princeton Plasma Physics Laboratory:

<http://www.pppl.gov/techreports.cfm>

Office of Scientific and Technical Information (OSTI):

<http://www.osti.gov/scitech/>

Related Links:

[U.S. Department of Energy](#)

[U.S. Department of Energy Office of Science](#)

[U.S. Department of Energy Office of Fusion Energy Sciences](#)

Ideal plasma response to vacuum magnetic fields with resonant magnetic perturbations in non-axisymmetric tokamaks

Kimin Kim

*Princeton Plasma Physics Laboratory, Princeton, NJ 08543, USA and
Korea Advanced Institute of Science and Technology, Daejeon 305-701, Korea*

J.-W. Ahn

Oak Ridge National Laboratory, Oak Ridge, TN 37831, USA

F. Scotti

Lawrence Livermore National Laboratory, Livermore, CA 94551, USA

J.-K. Park and J. E. Menard

Princeton Plasma Physics Laboratory, Princeton, NJ 08543, USA

(Dated: June 29, 2015)

Ideal plasma shielding and amplification of resonant magnetic perturbations in non-axisymmetric tokamak is presented by field line tracing simulation with full ideal plasma response, compared to measurements of divertor lobe structures. Magnetic field line tracing simulations in NSTX with toroidal non-axisymmetry indicate the ideal plasma response can significantly shield/amplify and phase shift the vacuum resonant magnetic perturbations. Ideal plasma shielding for $n = 3$ mode is found to prevent magnetic islands from opening as consistently shown in the field line connection length profile and magnetic footprints on the divertor target. It is also found that the ideal plasma shielding modifies the degree of stochasticity but does not change the overall helical lobe structures of the vacuum field for $n = 3$. Amplification of vacuum fields by the ideal plasma response is predicted for low toroidal mode $n = 1$, better reproducing measurements of strong striation of the field lines on the divertor plate in NSTX.

I. INTRODUCTION

Importance of resonant magnetic perturbation (RMP) by externally applied non-axisymmetric magnetic fields has been continuously emphasized for control of edge localized modes (ELMs) in tokamaks throughout the first demonstration of ELM suppression on DIII-D [1] and the successes in other devices [2–4]. It has been a well-known explanation that the RMP forms stochastic transport layers at the pedestal and enhances particle transport to keep the plasma marginally inside ELM stability boundary. Formation of the stochastic layers by RMP has been well elucidated so far using vacuum field approximation ignoring plasma response to the non-axisymmetric fields.

Plasmas in tokamaks, however, respond to the applied non-axisymmetric magnetic fields by driving perturbed plasma currents, which induce perturbed magnetic fields to either amplify or shield the applied fields [5–8]. That is, perturbed magnetic field structure in practice can be significantly changed. The shielding of RMP has been widely studied and understood as plasma flow effects shielding the RMP penetration into plasmas. A lot of efforts have been made to understand such plasma response to internal and/or external magnetic perturbations in tokamaks and helical systems including stellarators [9–13]. There are models describing plasma response, developed to calculate stochastic field structure with or without finite plasma resistivity [14–18], however, final solution of perturbed equilibria strongly depends on the model used [18]. It is still underway to achieve a complete

solution of the perturbed equilibria including nonideal and nonlinear MHD processes, and the plasma response must be properly considered in the RMP studies to better understand underlying physics mechanism of stochastic transport and ELM control.

In this paper, we study the stochastic layer structure in the perturbed tokamak using the vacuum field approximation and the perturbed equilibrium with ideal plasma response. A main focus of this paper is to qualify the stochastic features of the ideal perturbed equilibrium compared to the vacuum field. We use a full ideal plasma response calculation to achieve the total perturbed field for field line tracing simulations, and show the plasma response can significantly modify the characteristics of magnetic field structure in the presence of the non-axisymmetric magnetic fields. For low n experiments like $n = 1$, it is found that field line tracing simulations employing full ideal plasma response in this work may better explain the divertor footprint observations.

II. FIELD LINE TRACING SIMULATION

The field line tracing simulation is a well-known tool to study the stochastic magnetic field structure in the non-axisymmetric magnetic perturbations. It is useful to display and investigate the formation and modification of stochastic layers by the non-axisymmetric perturbations [4, 19–21]. A new field line tracing routine is used in this study, which has been implemented in the POCA code

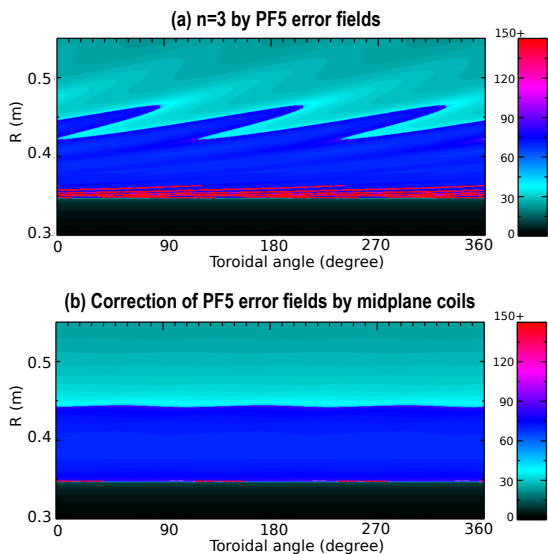


FIG. 1: Contour plot of field line connection length for (a) $n = 3$ PF5 error fields and (b) correction of the error fields using error field correction coils in NSTX. These contours indicate (a) striation of the field lines by the intrinsic error fields and (b) correction of the error fields.

[22–24] by solving a set of magnetic differential equations

$$\frac{\partial R}{\partial \phi} = \frac{RB_R}{B_\phi}, \quad \frac{\partial Z}{\partial \phi} = \frac{RB_Z}{B_\phi}.$$

Here, (B_R, B_Z, B_ϕ) are the magnetic field strength on the cylindrical coordinates (R, Z, ϕ) . The field line tracing routine, called POCA-FLT, solves the magnetic differential equations in the realistic tokamak geometry including the plasma facing components such as divertor, limiter and wall structures, as well as separatrix. This simulation provides various output information for a given non-axisymmetric magnetic field, such as field line connection length, field line loss fraction, Poincare map at the prescribed toroidal angle, and magnetic footprint on the divertor plate covering full toroidal angle. The POCA-FLT code is similar to other existing field line tracing codes in general, however, it has convenient features designed to study the physics of plasma response through a coupling to the ideal perturbed equilibrium code, IPEC [25]. The IPEC code provides POCA-FLT the perturbed magnetic field information calculated with the vacuum field approximation and the ideal plasma response.

One feature is that POCA-FLT can separately track the perturbed magnetic field lines produced by intrinsic error fields in NSTX, which are extracted by IPEC run. The error field effects can be independently studied without non-axisymmetric field coils. Typical simulation results are shown in Fig. 1, where the magnetic footprints on the divertor target are drawn by contour plots of field line connection length for an error field correction discharge in NSTX. The field line connection length is calculated by tracking a magnetic field line for 200

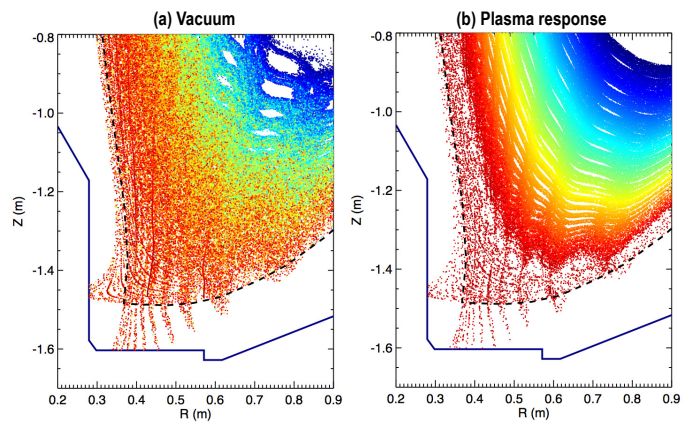


FIG. 2: Poincare map of the magnetic field lines with (a) vacuum approximation and (b) ideal plasma response computed by IPEC with $\psi_{\text{lim}} = 0.97$. Broken line indicates separatrix of the axisymmetric equilibrium.

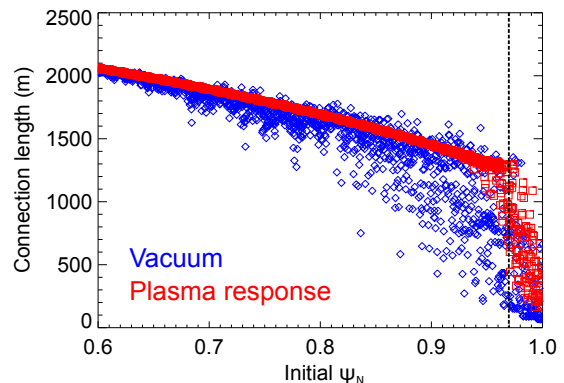


FIG. 3: Field line connection length profile with the vacuum field approximation and the ideal plasma response as a function of initial ψ_N . Vertical broken line indicates the boundary of the ideal plasma at $\psi_{\text{lim}} = 0.97$.

toroidal turns in co- and counter- I_p directions until the field line touches plasma facing components. This is a useful parameter that can be compared with camera images on the divertor (Figs. 4, 7) since large connection length implies the field lines stay in the hot plasma core for longer time to carry high heat fluxes [26]. Fig. 1(a) is the footprint by intrinsic $n = 3$ error fields from PF5 coils [27, 28] without applying the non-axisymmetric coil currents, and 1(b) is the one by combined fields of the PF5 error fields and correction fields supplied by the mid-plane error field correction coils in NSTX. Here, n is the toroidal mode number. As seen in the figure, the PF5 intrinsic error fields create helical lobe structures represented by typical striation patterns of $n = 3$ mode. However, Fig. 1(b) indicates that the helical lobes disappear when the correction fields are applied by the error field correction coils, as achieved in the experiment. The separate treatment of the error fields would be useful to investigate observations of the lobes even without mid-plane coil currents in several NSTX discharges.

Another feature is that the POCA-FLT simulation can fully take into account the ideal plasma response that shields the normal resonant field at the rational surfaces [29]. Such capability is important since the plasma response plays a crucial role in forming and altering the stochastic layers as reported in Refs. [30, 31], where a helical current sheets model aligned with the external field was applied to represent the screening of the resonant magnetic perturbations. The POCA-FLT performs the field line tracing in a similar manner but employs a full ideal plasma response calculation by IPEC.

III. SHIELDING OF VACUUM FIELD BY IDEAL PLASMA RESPONSE

One can find that the stochasticity is significantly modified by the ideal plasma shielding in the Poincare maps in Fig. 2, where $n = 3$ non-axisymmetric field was applied using the midplane coils in NSTX. The same colors in the contour indicate the same initial flux surfaces where tracking of the field line begins (i.e., core: blue, edge: red). There is one free parameter ψ_{lim} , the computational boundary of ideal plasma in the simulation; IPEC code computes the perturbed equilibria with the ideal plasma up to a certain normalized poloidal flux ψ_{lim} . The volume outside ψ_{lim} is treated as vacuum, but overall force balance is still maintained.

Fig. 2(a) shows a Poincare map with typical $n = 3$ helical lobe structure generated by the midplane coils in NSTX using the vacuum fields. Splitting of the field lines towards the divertor plate is consistent with an observation of the split striking points in NSTX [21]. Islands open on the rational flux surfaces by the resonant field components, and overlap to form the stochastic layers in the whole region. On the other hand, the stochasticity is largely changed by inclusion of the ideal plasma response with $\psi_{\text{lim}} = 0.97$ as shown in Fig. 2(b). The stochastic layers formed inside ψ_{lim} by the vacuum fields disappear due to shielding of resonant field components. Magnetic islands are not opened in the inner region but altered to make a wobble-like structure on the flux surfaces, which is identical to the perturbed flux surface. However, islands reopen due to unshielded resonant components in the vacuum region outside ψ_{lim} , thus stochasticity arises again to create almost identical helical lobes to the ones predicted by the vacuum fields. It should be noted that the wobble-like structure in Fig. 2(b) is due to the current sheet at the rational surfaces driven by the ideal plasma response in this simulation. Such shielding effects are not guaranteed in the presence of nonideal plasma response with finite resistivity.

One can see the modification of stochasticity more clearly in Fig. 3, where field line connection length profiles are plotted for the same case in Fig. 2. Note the x-axis is not the radial position of the Poincare map in Fig.2 but the initial normalized poloidal flux where tracing the field lines begins. The connection length in

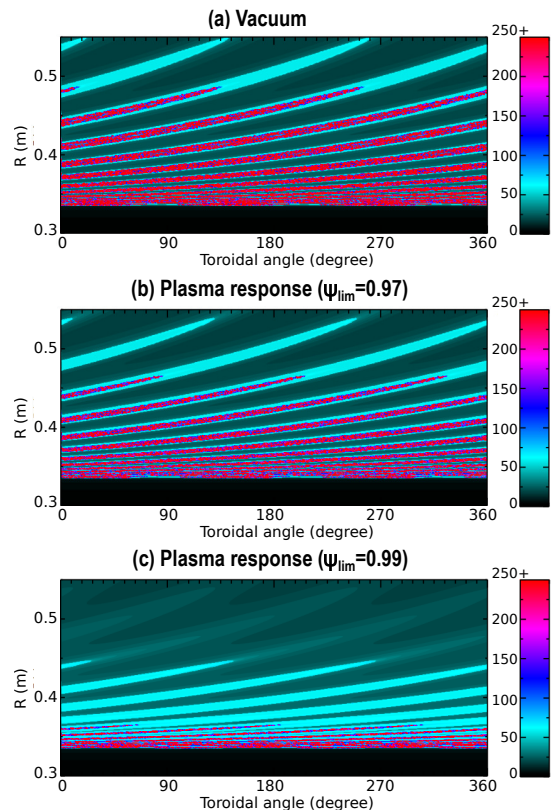


FIG. 4: Contour plot of field line connection length by $n = 3$ non-axisymmetric field with (a) the vacuum field approximation and the ideal plasma response of (b) $\psi_{\text{lim}} = 0.97$, and (c) $\psi_{\text{lim}} = 0.99$. Increasing ψ_{lim} leads to weaker striations.

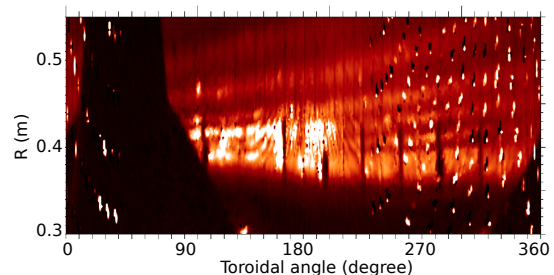


FIG. 5: Wide angle visible camera image to be compared with Fig. 4.

the vacuum field is found to be shorter than the ideal plasma response case on the rational surfaces because island overlapping moves out the field line fast. Therefore, the connection length profile appears stochastic as well. However, field lines are well-confined by the ideal plasma shielding, thus the connection length becomes an almost continuous function inside ψ_{lim} . The ideal plasma shielding causes an amplification of plasma currents and thereby amplification of the perturbed field outside the ideal plasma boundary to maintain the force balance. This is consistent with the increased connection length outside the boundary. It should be noted that a slight

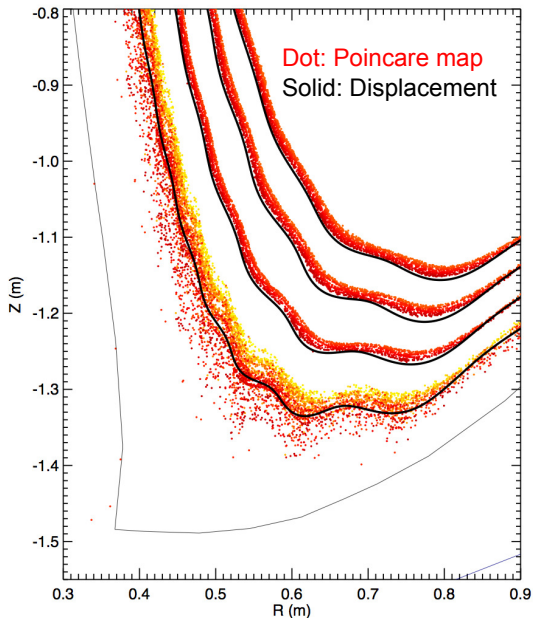


FIG. 6: Poincare plot of the field line tracing simulation including the ideal plasma response ($\psi_{\text{lim}}=0.97$), compared to the perturbed flux surface constructed with ideal plasma displacements computed by IPEC.

inside of ψ_{lim} in the ideal case is stochastic, however, it does not mean the ideal plasma response breaks the magnetic flux conservation. As noted earlier, since the x-axis of Fig. 3 is the initial flux surface for the field line tracing, the stochastic layer inside of ψ_{lim} indicates flux lines on those surfaces can be connected to vacuum layer due to the wobble-like structure in the vicinity of ideal plasma boundary as shown in Figs. 2b and 6. This mixes the ideal plasma and the vacuum layers, and self-consistent models will be required in the future to better understand such complicated mixed structures.

Effects of the ideal boundary ψ_{lim} can be quantitatively examined with magnetic footprints. Fig. 4 (a-c) are contour plots of field line connection length for the vacuum and the ideal perturbed equilibrium with $\psi_{\text{lim}} = 0.97$ and 0.99 for the same case in Fig. 2. The vacuum case in Fig. 4(a) is striations of field lines on the target produced by $n = 3$ vacuum field, showing consistent patterns with the observation by a wide angle visible camera in Fig. 5 [32], where neutral lithium emission is used to image striations on the lower divertor plasma facing components [33]. Fig. 4(b) with $\psi_{\text{lim}} = 0.97$ shows similar but weaker striations due to the shielding of resonant field components. Pushing the ideal plasma region to $\psi_{\text{lim}} = 0.99$ makes the footprints even weaker due to stronger shielding effects in Fig. 4(c). Simulation results indicate the plasma may respond to the externally applied field to modify the stochasticity in the non-axisymmetric magnetic perturbations. A quantitative comparison between extended numerical models and divertor heat flux measurement will be further required for validating plasma

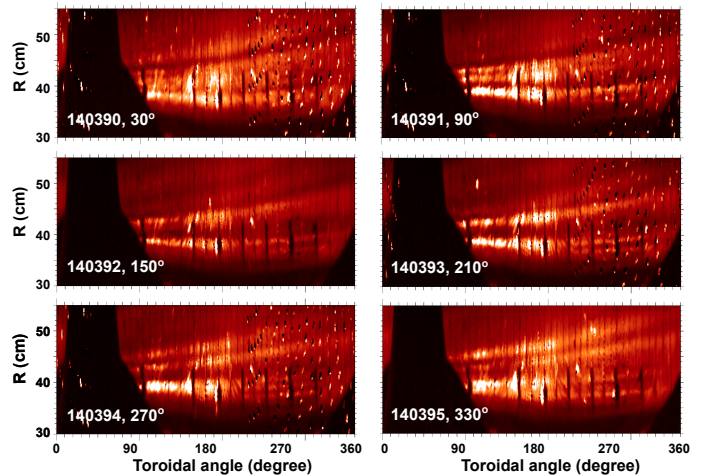


FIG. 7: Wide angle camera images of divertor lobe structure for experiments scanning footprint with $n = 1$ phase angle. Strong and static striations were observed regardless of the coil phase angle.

response models and understanding underlying physics.

Defining the perturbed flux surfaces of the perturbed equilibria is one issue to be resolved. The perturbed flux surface can be established by normal plasma displacement in the ideal MHD, while it can be also obtained from the Poincare map in the field line tracing or contours of the perturbed electron temperature in the resistive approach [18]. Fig. 6 is a direct comparison of the perturbed flux surfaces between the Poincare map of field lines with ideal plasma response and the normal displacement computed by IPEC. The solid curves in the figure are the superposition of normal displacements on the axisymmetric flux surfaces. It is found that the perturbed flux surfaces from the ideal displacements agree with the wobble-like structures of Poincare plot in the ideal plasma region, as pronounced by a relation between the perturbed magnetic field and the displacement ξ by $\delta\vec{B} = \nabla \times (\xi \times \vec{B}_0)$ in the ideal MHD theory. However, the magnetic field lines are stochastic around the ideal plasma boundary, so the perturbed flux surfaces cannot be well defined from the vacuum approximation.

IV. AMPLIFICATION OF VACUUM FIELD BY IDEAL PLASMA RESPONSE

Plasmas can respond to the applied non-axisymmetric fields to amplify and/or phase shift the perturbations [29]. The midplane non-axisymmetric field coils in NSTX are capable of applying the $n = 1$ perturbations in the six phase angle, providing toroidally phase shifted $n = 1$ fields depending on the angle. Modification of magnetic field line structure by the $n = 1$ magnetic perturbations has been investigated using a series of discharges measuring helical lobe structure by the $n = 1$ fields in the six coil phases. The wide angle visible camera has used

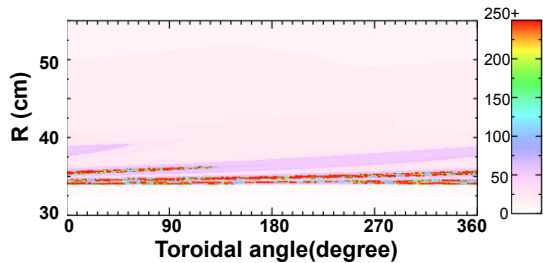


FIG. 8: Divertor footprint by typical $n = 1$ perturbation, obtained from connection length in field line tracing simulation using vacuum fields. Much weaker striation than measurement was computed.

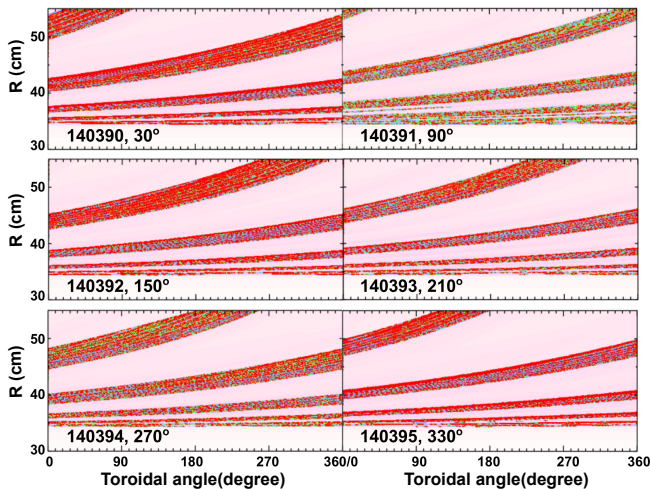


FIG. 9: Divertor footprints by $n = 1$ fields for each coil phase angle, calculated by field line tracing simulations including ideal plasma response. Strong striations were reproduced due to amplification of vacuum fields, giving much better agreement with measurements.

to image the footprints of magnetic field lines on the divertor plate for each discharge, which are summarized in Fig. 7. General expectation was that phase angle shift of the coils will produce toroidally phase-shifted striation patterns corresponding to the shifted $n = 1$ field. However, as shown in the Fig. 7, two interesting points were observed in the experiments; First, strong striations in the helical lobe structure are captured in every discharge. Second, measured lobe structures does not show a clear phase-shift of the patterns in spite of the phase angle shift between the discharges.

Vacuum field line tracing simulations have been tried to understand the experimental observation, and it was found that the vacuum field approximation ignoring the plasma response was not valid for these experiments. The vacuum field line tracing simulation result for the $n = 1$ 30 degree case (140390) is shown in Fig. 8 as an example. It is clear that experimentally measured strong striation of the footprint pattern cannot be achieved by the vacuum fields even though every possible field component of

NSTX was included in the calculation (e.g., $n = 1$ and $n = 3$ components from midplane, PF5, and TF coils). On the other hand, clear toroidal rotation of the footprint patterns due to the phase angle shift was obtained in the calculations (not shown). Unlike the $n = 3$ cases, vacuum field line tracing was not able to reproduce and explain neither of strong striation and static patterns presented in the wide angle camera images in Fig. 7.

It is implied that the vacuum fields should be amplified and phase shifted to narrow the discrepancies between observations and calculations and the plasma response may be responsible for the field modification. We consider the ideal plasma response calculation and equilibrium reconstruction using kinetic EFIT. The kinetic EFIT including steep pedestal structure and strong contribution of bootstrap current was utilized for IPEC and POCA-FLT computations, where edge safety factor and its shear profile strongly impacted on both axisymmetric and non-axisymmetric equilibriums. Calculation results with combining ideal plasma and kinetic EFIT are presented in Fig. 9. They indicate that modification of the applied non-axisymmetric fields by ideal plasma response dramatically amplified the amplitudes of vacuum $n = 1$ fields and produced more consistent divertor footprints to the camera image. The ideal plasma response was found to significantly modify the envelope of lobes of vacuum fields unlike $n = 3$ cases, therefore, striation patterns were also significantly changed from the ones by vacuum fields. Overall field line tracing simulations including the ideal plasma response provide much better agreement with the camera images.

One can notice that some local discrepancies between measurements and calculations still remain. Measurements show that almost stationary footprint patterns were created in the discharges despite the phase angle change, even though rotation of vacuum $n = 1$ fields may have to produce toroidally rotating footprint patterns. Field line tracing simulations with ideal plasma response present partially stationary and partially rotating footprint patterns, as presented by discontinuities of lobe structures between discharges in the simulation. Footprints by externally applied $n = 1$ fields rotate toroidally, however, the amplification of intrinsic error fields by the ideal plasma response included in the simulations for Fig. 9 compensates such rotating effects and produces partially stationary striation patterns.

Note strong amplifications of $n=1$ fields cause a significant mixing of the ideal plasma and the vacuum layers as stated in Sec. 3. They produce significant amount of new field line connections from edge to divertor plates that are not captured in the vacuum field line tracing, and modify footprint shapes on the divertor plates. Inclusion of other error field sources makes the pattern by the ideal plasma response look more different from vacuum field case. They can look even more different especially when the field sources are complicated across intrinsic and applied components with different toroidal modes.

More evidences will be required to confirm that the

ideal plasma response is solely responsible for the diverter footprints in the $n = 1$ magnetic perturbations on NSTX. Instead, it would be possible to argue that the ideal plasma response can play significant roles in modifying the magnetic field structure, which better explains the $n = 1$ experiments of NSTX. It is also clear that self-consistent non-axisymmetric equilibria is necessary for better understanding of observations. Since plasmas in reality are non-ideal and lie somewhere between ideal and vacuum regimes, ideal or vacuum model can be a good approximation depending on the discharges. However, more advanced plasma response model must be taken into account to achieve full physical mechanism of the non-axisymmetric perturbed equilibria in tokamaks. Ideal plasma response model can be one approach as shown in this paper, however, robust and complete models including non-ideal effects should be studied and cross-benchmarked.

V. CONCLUSIONS

Field line tracing simulations using POCA-FLT code show that ideal plasma response can shield or amplify

the externally applied vacuum non-axisymmetric magnetic fields. Simulation results found the ideal plasma response shielding of $n = 3$ vacuum fields and amplification of $n = 1$ fields, implying vacuum fields can be significantly modified in amplitude and phase by the plasma response. Impacts of plasma response will be even more complicated in the presence of non-ideal and nonlinear MHD processes. Inclusion of such rich physics remains as a future work. It is clearly indicated in this study that the plasma response must be taken into account in the non-axisymmetric tokamak physics study to better understand the stochastic plasma transport and ELM suppression, which eventually will require a self-consistent perturbed equilibria.

Acknowledgments

This work was supported by DOE Contract DE-AC02-09CH11466 (PPPL) and DE-AC52-07NA27344 (LLNL). Part of the work was supported by the National Research Foundation of Korea (NRF) funded by the Ministry of Science, ICT and Future Planning (NRF-2014M1A7A1A03045092).

-
- [1] T. E. Evans, R. A. Moyer, P. R. Thomas, J. G. Watkins, T. H. Osborne, J. A. Boedo, E. J. Doyle, M. E. Fenstermacher, K. H. Finken, R. J. Groebner, et al., *Phys. Rev. Lett.* **92**, 235003 (2004).
 - [2] W. Suttrop, T. Eich, J. C. Fuchs, S. Günter, A. Janzer, A. Herrmann, A. Kallenbach, P. T. Lang, T. Lunt, M. Maraschek, et al., *Phys. Rev. Lett.* **106**, 225004 (2011).
 - [3] Y. M. Jeon, J.-K. Park, S. W. Yoon, W. H. Ko, S. G. Lee, K. D. Lee, G. S. Yun, Y. U. Nam, W. C. Kim, J.-G. Kwak, et al., *Phys. Rev. Lett.* **109**, 035004 (2012).
 - [4] A. Kirk, J. Harrison, Y. Liu, E. Nardon, I. T. Chapman, P. Denner, and the MAST team, *Phys. Rev. Lett.* **108**, 255003 (2012).
 - [5] A. H. Boozer, *Phys. Rev. Lett.* **86**, 5059 (2001).
 - [6] A. H. Boozer and C. Nührenberg, *Phys. Plasmas* **13**, 102501 (2006).
 - [7] M. J. Lanctot, H. Reimerdes, A. M. Garofalo, M. S. Chu, Y. Q. Liu, E. J. Strait, G. L. Jackson, R. J. L. Haye, M. Okabayashi, T. H. Osborne, et al., *Phys. Plasmas* **17**, 030701 (2010).
 - [8] M. S. Chu, L. L. Lao, M. J. Schaffer, T. E. Evans, E. J. Strait, Y. Q. Liu, M. J. Lanctot, H. Reimerdes, Y. Liu, T. A. Casper, et al., *Nucl. Fusion* **51**, 073036 (2011).
 - [9] R. Fitzpatrick, *Nucl. Fusion* **33**, 1049 (1993).
 - [10] M. Bécoulet, G. Huysmans, X. Garbet, E. Nardon, D. Howell, A. Garofalo, M. Schaffer, T. Evans, K. Shaing, A. Cole, et al., *Nucl. Fusion* **49**, 085011 (2009).
 - [11] Y. Narushima, F. Castejon, S. Sakakibara, K. Y. Watanabe, S. Ohdachi, Y. Suzuki, T. Estrada, F. Medina, D. Lopez-Bruna, M. Yokoyama, et al., *Nucl. Fusion* **51**, 083030 (2011).
 - [12] C. C. Hegna, *Nucl. Fusion* **51**, 113017 (2011).
 - [13] S. Nishimura, S. Toda, M. Yagi, and Y. Narushima, *Phys. Plasmas* **19**, 122510 (2012).
 - [14] A. H. Boozer, *Phys. Plasmas* **13**, 044501 (2006).
 - [15] J.-K. Park, M. J. Schaffer, J. E. Menard, and A. H. Boozer, *Phys. Rev. Lett.* **99**, 195003 (2007).
 - [16] Y. Liu, A. Kirk, Y. Gribov, M. P. Gryaznevich, T. C. Hender, and E. Nardon, *Nucl. Fusion* **51**, 083002 (2011).
 - [17] N. M. Ferraro, T. E. Evans, L. L. Lao, R. A. Moyer, R. Nazikian, D. M. Orlov, M. W. Shafer, E. A. Unterberg, M. R. Wade, and A. Wingen, *Nucl. Fusion* **53**, 073042 (2013).
 - [18] A. D. Turnbull, N. M. Ferraro, V. A. Izzo, E. A. Lazarus, J.-K. Park, W. A. Cooper, S. P. Hirshman, L. L. Lao, M. J. Lanctot, S. Lazerson, et al., *Phys. Plasmas* **20**, 056114 (2013).
 - [19] T. E. Evans, R. A. Moyer, and P. Monat, *Phys. Plasmas* **9**, 4957 (2002).
 - [20] M. W. Jakubowski, T. E. Evans, M. E. Fenstermacher, M. Groth, C. J. Lasnier, A. W. Leonard, O. Schmitz, J. G. Watkins, T. Eich, W. Fundamenski, et al., *Nucl. Fusion* **49**, 095013 (2009).
 - [21] J.-W. Ahn, R. Maingi, J. M. Canik, A. G. McLean, J. D. Lore, J.-K. Park, V. A. Soukhanovskii, T. K. Gray, and A. L. Roquemore, *Phys. Plasmas* **18**, 056108 (2011).
 - [22] K. Kim, J.-K. Park, G. J. Kramer, and A. H. Boozer, *Phys. Plasmas* **19**, 082503 (2012).
 - [23] K. Kim, J.-K. Park, and A. H. Boozer, *Phys. Rev. Lett.* **110**, 185004 (2013).
 - [24] K. Kim, J.-K. Park, A. H. Boozer, J. E. Menard, S. P. Gerhardt, N. C. Logan, Z. R. Wang, G. J. Kramer, K. H. Burrell, and A. M. Garofalo, *Nucl. Fusion* **54**, 073014 (2014).
 - [25] J.-K. Park, A. H. Boozer, and A. H. Glasser, *Phys. Plas-*

- mas **14**, 052110 (2007).
- [26] A. Wingen, T. E. Evans, and K. H. Spatschek, *Phys. Plasmas* **16**, 042504 (2009).
- [27] S. P. Gerhardt, J. E. Menard, J.-K. Park, R. Bell, D. A. Gates, B. P. Le Blanc, S. A. Sabbagh, and H. Yuh, *Plasma Phys. Control. Fusion* **52**, 104003 (2010).
- [28] J. E. Menard, R. E. Bell, D. A. Gates, S. P. Gerhardt, J.-K. Park, S. A. Sabbagh, J. W. Berkery, A. Egan, J. Kallman, S. M. Kaye, et al., *Nucl. Fusion* **50**, 045008 (2010).
- [29] J.-K. Park, A. H. Boozer, J. E. Menard, S. P. Gerhardt, and S. A. Sabbagh, *Phys. Plasmas* **16**, 082512 (2009).
- [30] P. Cahyna, E. Nardon, and JET EFDA Contributors, *J. Nucl. Mater.* **415**, S927 (2011).
- [31] H. Frerichs, D. Reiter, O. Schmitz, P. Cahyna, T. E. Evans, Y. Feng, and E. Nardon, *Phys. Plasmas* **19**, 052507 (2012).
- [32] J.-W. Ahn, F. Scotti, K. Kim, J. M. Canik, J. D. Lore, R. Maingi, A. G. McLean, R. E. Bell, A. Diallo, S. P. Gerhardt, et al., *Plasma Phys. Control. Fusion* **56**, 015005 (2014).
- [33] F. Scotti, A. Roquemore, and V. A. Soukhanovskii, *Rev. Sci. Instrum.* **83**, 10E532 (2012).

Princeton Plasma Physics Laboratory Office of Reports and Publications

Managed by
Princeton University

under contract with the
U.S. Department of Energy
(DE-AC02-09CH11466)

P.O. Box 451, Princeton, NJ 08543
Phone: 609-243-2245
Fax: 609-243-2751

E-mail: publications@pppl.gov

Website: <http://www.pppl.gov>